Weldability of cold-formed high strength and ultra-high strength steels

Afkhami Shahriar, Björk Timo, Larkiola Jari

DOI: 10.1016/j.jcsr.2019.03.017

Accepted Manuscript

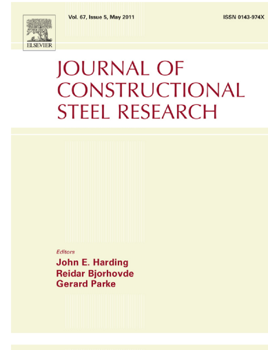

Weldability of cold-formed high strength and ultra-high strength steels

Shahriar Afkhami, Timo Björk, Jari Larkiola

PII: S0143-974X(18)30935-0
DOI: https://doi.org/10.1016/j.jcsr.2019.03.017
Reference: JCSR 5546

To appear in: *Journal of Constructional Steel Research*

Received date: 5 September 2018
Revised date: 4 January 2019
Accepted date: 13 March 2019

Please cite this article as: S. Afkhami, T. Björk and J. Larkiola, Weldability of cold-formed high strength and ultra-high strength steels, Journal of Constructional Steel Research, https://doi.org/10.1016/j.jcsr.2019.03.017

WELDABILITY OF COLD-FORMED HIGH STRENGTH AND ULTRA-HIGH STRENGTH STEELS

Shahriar Afkhami[a]; Timo Björk[a]; Jari Larkiola[b]

[a] Laboratory of Steel Structures, Lappeenranta University of Technology, P.O. Box 20, 53851, Lappeenranta, Finland

[b] Materials and Production Engineering, Faculty of Technology, University of Oulu, Box 4200, 90014, Oulu, Finland

Corresponding author: shahriar.afkhami@lut.fi

Abstract:

Hollow sections and cold-formed steels have a key role in modern structures and machinery. In addition, to benefit from full potentials of cold-formed steels, it is usually required to weld them to other steel parts of structures. However, data provided by relevant standards, such as Eurocode 3, do not cover newly developed high strength and ultra-high strength grades of this material. Thus, further study is critical to complete available data in literature and standards. Regarding this matter, having a good weldability for cold-formed high and ultra-high strength steels is vital for development of contemporary steel structures. Thus, newly developed steels S700MC and S1100 were selected to be investigated in this study. To do so, bended base metals with different degrees of cold-forming were welded to their straight (virgin) counterparts. Next, welded joints were investigated via microstructural analysis, hardness measurement, tensile test, and Charpy impact test to assess the weldabilities of the cold-formed base metals. Results show that the final joints had acceptable characteristics, and the cold-formed base metals showed good weldability. However, bending and pre-straining criteria recommended by the manufacturer must be satisfied to have an acceptable joint after welding. Beyond that criteria, fracture elongation and notch toughness of the welded joints decreased, and some welded samples failed from their cold-formed base metals.

Keywords: Ultra-high strength steel; Cold-formed; Weldability; S700MC; S1100

1. Introduction

Manufacturing of steel structures, as a resource-intensive industry, consumes high volumes of natural resources and introduces various types of waste materials into the environment. To minimize these negative effects, material preservation and sustainable production must be considered in the contemporary industry [1]. To do so, one effective approach is to use stronger materials; however, this is not always an efficient solution, since stronger and more advanced materials are usually costly. One way to use these materials and have an economic final product simultaneously is to use high strength steels (HSS) and ultra-high strength steels (UHSS). These steels provide a cost-effective solution for material preservation, manufacturing of strong and economic steel structures, and saving energy [2]. In addition, these steels contribute to a more sustainable construction by increasing the durability of the final product [1].

Ultra-high strength steels can be defined as a type of advanced high strength steels (AHSS) with a multiphase microstructure, which obtain a good combination of strength and ductility by grain refinement and thermomechanical processing. In addition, UHSSs and HSSs are considered as members of high strength low alloy (HSLA) steels due to their strength levels and low alloy contents [3, 4]. Microstructures of HSSs and UHSSs usually consist of a combination of irregular ferrite, bainite, martensite, and retained austenite [5]. Regarding their strength, although these steels have become more common in various industries, a general definition of strength range is not assigned to UHSSs yet. This lack of definition might be due to the constant development of these steels. Currently, the upper limit of yield strength for commercial grades of UHSSs has reached 1400 MPa, and it is getting higher progressively [4]. In this study, according to difinitions provided by [6], AHSS with the yield strength lower than 780 MPa are refered as HSSs, while stornger steels are considered as UHSSs.

To benefit from full potentials of HSSs and UHSSs and provide designers with more freedom, it is usually crucial to weld these steels. Thus, welding HSSs and UHSSs, especially by laser welding (LW) and gas-metal arc welding (GMAW), has been the subject of numerous studies [7]. In addition, weldability of these steels was investigated using various welding processes (including LW [8-10], ultra-narrow gap laser welding [11, 12], tungsten inert gas welding [13, 14], GMAW [12], and hybrid welding [15]) under different conditions (such as dissimilar welding positions [9] or dissimilar joints [16]).

According to studies carried out on the weldability of HSSs and UHSSs, common defects and difficulties associated with their welding are cold cracking [10, 17], decrease in toughness [18], lack of ductility [16], decrease in strength [12, 13], and softening of heat affected zone (HAZ) [8, 10, 18, 19]. However, it is usually possible to reduce these defects by controlling heat input, cooling rate, and heat flow during a welding procedure [14, 20].

HAZ softening and decrease in strength can be minimized via controlling heat input and using a proper welding process [11, 12, 15]. According to some studies, the best method to alleviate such effects is to control HAZ microstructure by using the least possible value of welding heat input and facilitate the heat dissipation away from the joint [20-22]. In addition, it is feasible to decrease the risk of cold cracking by controlling the humidity during the welding process, e.g. using a shielding gas [17].

In addition to welding, another way to improve the applicability of HSSs and UHSSs as well as to increase their strength to weight ratio is using their hollow sections. Cold-formed or tubular hollow sections are currently used to enhance the efficiency of steel structures, especially in construction and car manufacturing [23]. Furthermore, these hollow sections are critical for energy absorbent parts in the contemporary automobile industry. In addition, these sections increase safety, reduce weight, and decrease fuel consumption of modern vehicles [24]. However, none of these is possible without joining these sections into each other and other parts of structures. Among various joining processes, welding is one of the most effective and common methods. These points establish the importance of welded cold-formed HSSs and UHSSs in today's industry [2, 24, 25].

One drawback of cold-forming is the development of pre-strains in deformed steel and consequently in the hollow section made from it. These pre-strains can introduce new challenges into the welding of this material. Even a controlled amount of pre-strain changes mechanical properties of steel. This plastic deformation induces different degrees of permanent distortion on the microstructure. Additionally, it increases the dislocation density throughout the deformed microstructure. Excessive dislocations hinder grain boundaries movement and grains deformation while encouraging the mobility of atoms [26, 27]. These phenomena cause some changes in material behaviour, including an increase in its strength and hardness, a decrease in its ductility, and a drop in its fracture toughness. In addition, pre-strains may ease crack initiation and growth. Furthermore, they may increase ductile to brittle transition temperature (DBTT). Thus, cold-formed HSSs and UHSSs, such as their hollow sections, can show weldabilities different from those of their virgin (without pre-strain) materials [28-30].

This study aims to investigate weldability of cold-formed S700MC, as a frequently used HSS in steel structures, and S1100, as a newly developed UHSS. The main motivation of this research is the significant role of welded cold-formed HSSs and UHSSs in modern steel structures, especially pressure vessels, vehicles, and cranes [31-33]. Due to this important role, some studies investigated the welding and joint characteristics of HSSs and UHSSs under different conditions, including welding their cold-formed sections [20, 34-36]. Although some rules are presented for welding the cold-formed areas of steels by various standards, including EN 1993-1-8, these rules are limited to normal and some high strength steels. Thus, welding of cold-formed UHSSs still requires further investigation. This is of utmost importance, since the load bearing capacity of a steel structure is usually limited to the durability of its critical joints [23]. Therefore, the aim of this study is to investigate weldability of cold-formed HSS S700MC and UHSS S1100, welded by GMAW as a commonly used welding process in steel structures, automobile manufacturing, and crane production.

2. Materials and procedure

Two sets of welded joints, one made from S700MC as the base material and the other one made from S1100, were investigated in this study. According to the materials manufacturer, S700MC is a hot-rolled HSS with a minimum yield strength of 700 MPa and an acceptable formability. S1100 is a hot-rolled UHSS with a minimum yield strength of 1100 MPa which is suitable for cold-forming. Recommended application for the both steels is production of load-bearing steel structures [37, 38]. Chemical compositions of S700MC and S1100 are presented in tables 1 and 2 respectively. Mechanical properties of these steels are presented in table 3.

C (max wt%)	Si (max wt%)	Mn (max wt%)	P (max wt%)	S (max wt%)	Al (max wt%)	Nb (max wt%)	V (max wt%)	Ti (max wt%)
0.120	0.210	2.100	0.020	0.010	0.015	0.090	0.200	0.150
CEV= 0.39 CET= 0.25								

Table 1. Chemical composition of S700MC [38].

C (max wt%)	Si (max wt%)	Mn (max wt%)	P (max wt%)	S (max wt%)	Cr (max wt%)	Cu (max wt%)	Ni (max wt%)	Mo (max wt%)	B (max wt%)
0.210	0.500	1.400	0.020	0.005	0.800	0.300	3.000	0.700	0.005
CEV= 0.70 CET= 0.40									

Table 2. Chemical composition of S1100 [38].

Steel grade	Thickness (mm)	Minimum yield strength (MPa)	Tensile strength (MPa)	Minimum elongation (%)	Minimum bendability for 90° (r/t)	Impact energy at -40°C (J)
S700MC	2-10	700	750-950	12	1.6	27
S1100	5-40	1100	1250-1550	10	3.0	27

Table 3. Mechanical properties of S700MC and S1100 at the ambient temperature and their notch toughness values [38].

Air bending was used to introduce different degrees of pre-strain to the cold-formed base metals. Different degrees of cold-forming (DOC) were emulated by using different radius to thickness ratios (*r*/*t*) for the bending trials. After that, GMAW, as a frequently used welding process for industrial applications, was utilized to perform the welding procedures. Bending and welding parameters are presented in tables 4 and 5 respectively. To have a comparison between the cold-formed and virgin materials, each bended plate was welded to its virgin counterpart.

Regarding the filler materials, S700MC was welded using a matching one commercially known as Böhler alform® 700-MC, while Böhler union X96 was used for the samples made from S1100, although it was an undermatching filler material. This was due to the fact that X96 is currently the only commercially available filler material with a yield strength close to the yield strength of the base metal [39].

Material	Bending Radius (mm)	*r*/*t*	Dimensions of the Plate prior to the bending (mm)	Degree of bending[1] (Degree)	Maximum bending force[2] (KN)	Punch Speed (mm/s)	Die opening (mm)
S700MC	5	0.50	200×100×10	90	1000	9.5	100
S700MC	10	1.00	200×100×10	90	1000	9.5	100
S700MC	15	1.50	200×100×10	90	1000	9.5	100
S700MC	20	2.00	200×100×10	90	1000	9.5	100
S1100	24	3.00	200×300×8	90	1000	9.5	140
S1100	26	3.25	200×300×8	90	1000	9.5	140
S1100	28	3.50	200×300×8	90	1000	9.5	140
S1100	30	3.75	200×300×8	90	1000	9.5	140
S1100	37	4.60	200×300×8	90	1000	9.5	140
S1100	40	5.00	200×300×8	90	1000	9.5	140

[1] Bending axis was perpendicular to the rolling direction
[2] Bending machine: Press brake Ursviken Optima 100

Table 4. General specifications of the bended samples and their bending parameters.

Base material	*r*/*t*	Welding voltage (V)	Welding Current (A)	Number of passes[1]	Travel speed (mm/s)	Approximate accumulated heat input (KJ/mm)	Type of the filler material	Type of the shielding gas
S700MC	0.50	25	220	3	7.5	1.75	Böhler alform® 700-MC	92%Ar-8%CO_2
S700MC	1.00	25	220	3	7.5	1.75	Böhler alform® 700-MC	92%Ar-8%CO_2
S700MC	1.50	25	220	4	7.5	2.50	Böhler alform® 700-MC	92%Ar-8%CO_2
S700MC	2.00	25	220	4	7.5	2.50	Böhler alform® 700-MC	92%Ar-8%CO_2
S1100	3.00	25	220	4	7.5	2.50	Böhler union X96	92%Ar-8%CO_2
S1100	3.25	25	220	4	7.5	2.50	Böhler union X96	92%Ar-8%CO_2
S1100	3.50	25	220	4	7.5	2.50	Böhler union X96	92%Ar-8%CO_2
S1100	3.75	25	220	4	7.5	2.50	Böhler union X96	92%Ar-8%CO_2
S1100	4.60	25	220	4	7.5	2.50	Böhler union X96	92%Ar-8%CO_2
S1100	5.00	25	220	4	7.5	2.50	Böhler union X96	92%Ar-8%CO_2

[1] Preheat temperature for all the welds: 25 °C
[1] The maximum interpass temperature for all the welds: 50 °C

Table 5. Welding parameters according to the bending conditions and base materials.

After welding, the samples were cut into proper size and polished to achieve required surface finish to perform microstructural analysis and microhardness measurements. The polished samples were etched by Nital (95 ml of C_2H_5OH + 5 ml of HNO_3) for 5 seconds for revealing their macrostructural and microstructural features. Macrostructural analysis of the samples was carried out via optical microscopy, while the microstructural features were studied by scanning electron microscopy (SEM). Prior to SEM, hardness measurements were carried out following ISO 6507-1 to recognize different zones (base metal, heat affected zone, and fusion zone) and sub-zones (HAZ sub-zones) for the microstructural analysis [40].

Regarding the uniaxial tensile test, flat specimens were cut out of the welded samples in accordance with ASTM E8M (figure 1.A) [41]. The tensile tests were carried out with a strain rate of 0.004 s^{-1}. During the trials, ARAMIS, as a digital image correlation (DIC) system, measured and recorded displacements to calculate the elongation values. In addition to the tensile test, Charpy impact test was carried out on the welded samples to have a more comprehensive evaluation of their mechanical properties.

Sub-size Charpy specimens were prepared according to ASTM E23M (figure 1.B), and their notch toughness values were measured at -40 °C. Due to the limited thickness of the welded samples, the thickness value of the specimens was set to 5 mm [42]. A correction factor calculated by equations 1 and 2 [43] was used to extrapolate actual notch toughness values. After breaking the samples, their fracture surfaces were analyzed via micro-photography to determine the shear fracture area (SFA). This parameter was used to estimate the ductile to brittle fracture ratio of each specimen.

$$e = \left[K \times \left(1 - \frac{d}{D}\right) + E \times \frac{d}{D}\right] \times \frac{s}{S} \tag{1}$$

Where e and E are the fracture energy densities (J/mm^3) of sub-size and normal specimens respectively. K is the rupture energy which is considered as 29.3 J for ductile steels. D and d are the ligament sizes of normal and sub-size specimens respectively (mm). Finally, s and S are the cross-sectional areas of sub-size and normal specimens respectively (mm^2). According to Lucon et al. [43], if sub-size and normal specimens have equal ligament sizes, similar to the specimens used in this study, their fracture energy densities are proportional to their cross-sectional areas. Thus, equation 1 can be modified to equation 2:

$$e = E \times \frac{s}{S} \qquad (2)$$

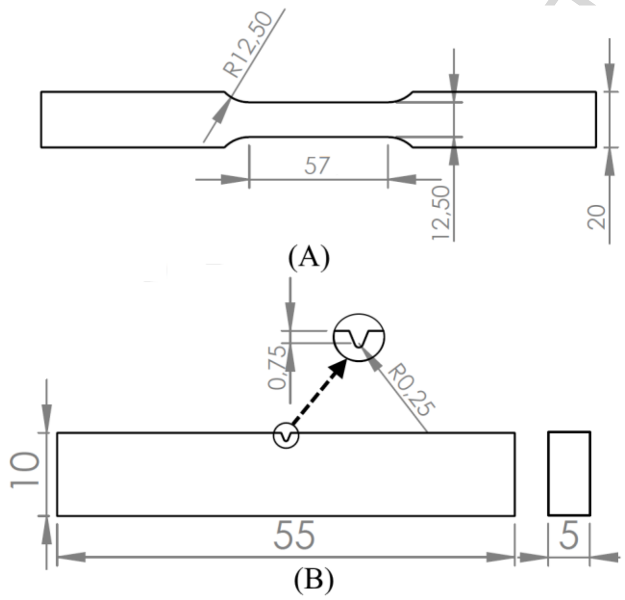

Figure. 1 Schematic view of the (A) flat tensile [41], and (B) sub-size notch toughness specimens [42].

3. Results and discussion

According to visual inspection of the welded samples, the welded joints did not have any type of defects and cracks. As an example, the macrostructural features of the samples with the lowest (5 mm) and the highest (40 mm) bending radii are presented in figure 2. According to this figure, bending process and its resultant pre-strains did not cause any macrostructural discontinuity and rupture prior to the welding trials. Furthermore, the welding procedure did not cause any type of defects in the joints.

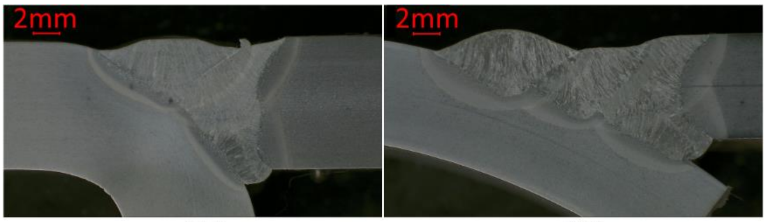

(A) (B)

Figure 2. Welded joints with the base material and the bending radius of (A) S700MC, 5 mm; (B) S1100, 40 mm.

3.1 Microstructures of the base metals

Microstructures of the base metals in their as-received condition are presented in figure 3. As can be seen in figure 3.A, the microstructure of S700MC consisted of a mixture of bainite and islands of martensite-austenite (M/A), which appeared as non-etched smooth blocks in this figure. In addition, according to Navarro-López et al. [44], etched areas with irregular shapes (as one of them is indicated with white dashed boundaries) were also of bainitic origin, although they had a smooth appearance. All these microstructural features were within packets extended to the prior austenite grain boundaries. Additionally, some small blocks were scattered along the prior austenite grain boundaries and between the bainite laths (indicated by white dashed arrows in figure 3.A). According to [44], these blocks were likely small islands of retained austenite entrapped between other phases, along their high-angle boundaries.

The microstructure of S1100 is presented in figure 3.B. As shown in this figure, this steel consisted of islands of M/A surrounded by bainite and ferrite. In addition, similar to S700MC, some small blocks of retained austenite (indicated by white dashed arrows) were scattered along the prior austenite grain boundaries and between the laths of bainite. As indicated in figure 4 by white dashed boundaries, by increasing the magnification to 10000×, an elongated morphology with wavy boundaries, including irregular patterns of sporadic carbides, also appeared beside the ferritic laths. According to Navarro-López et al. [44], this type of morphology has a martensitic origin and, due to the presence of scattered carbides with no specific direction, can be considered as tempered martensite.

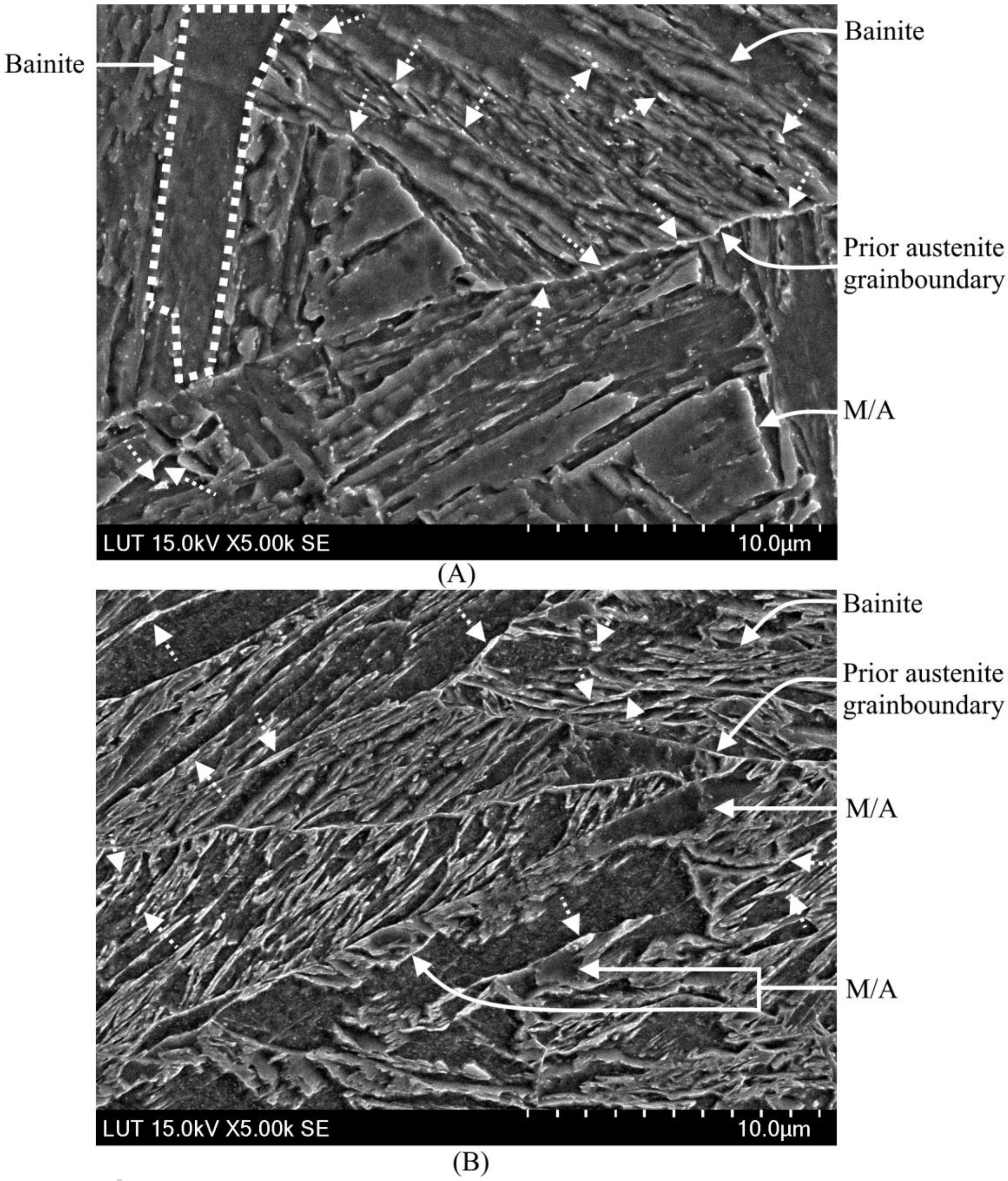

Figure 3. Microstructures of the base metals: (A) S700MC, (B) S1100.

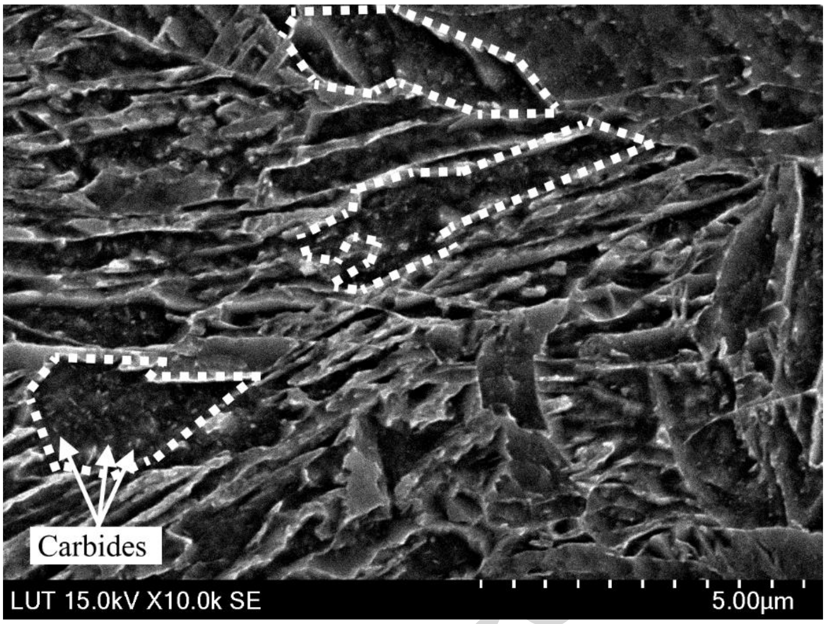

Figure 4. Microstructure of S1100 in 10000× magnification.

3.2 Hardness profiles and HAZ microstructures

Hardness profile of the welded sample made from S700MC with r/t= 2 is presented in figure 5. Hardness profiles of the other S700MC samples were similar to the data from this figure. According to figure 5, hardness values on the cold-formed side were slightly higher than their counterparts on the virgin side. This behaviour can be attributed to the higher dislocation density of the cold-formed material and its strain hardening [28, 29]. In addition, the middle section, as the most severely heated zone, had the lowest hardness value along its cross-sectional area. The entire HAZ was a mixture of bainite and martensite but their ratio, morphology, and roughness were different in every HAZ sub-zone. In addition, the average hardness of the weld metal (Böhler alform® 700-MC) was higher than the average hardness of the other zones. According to figure 6, this higher hardness was due to the fine-textured martensitic microstructure of this area.

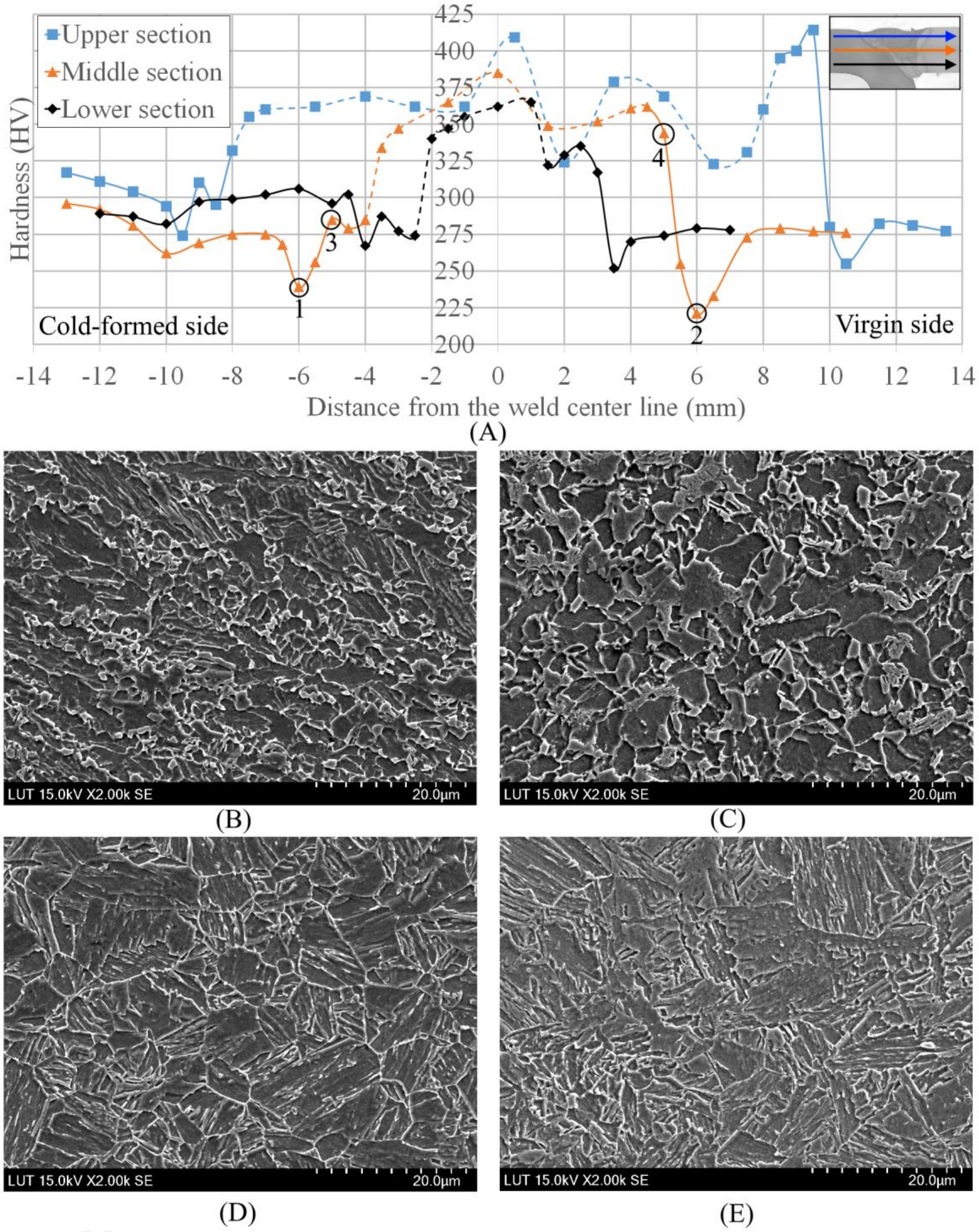

Figure 5. (A) Hardness profiles of S700MC with r/t=2 (area of the weld metal is indicated by dashed lines along the profiles); and its HAZ microstructures: (B) microstructure of the softened zone on the cold-formed side (point 1 in A); (C) microstructure of the softened zone on the virgin side (point 2 in A); (D) microstructure of the point with the highest hardness value on the cold-formed side (point 3 in A); (E) microstructure of the point with the highest hardness value on the virgin side (point 4 in A).

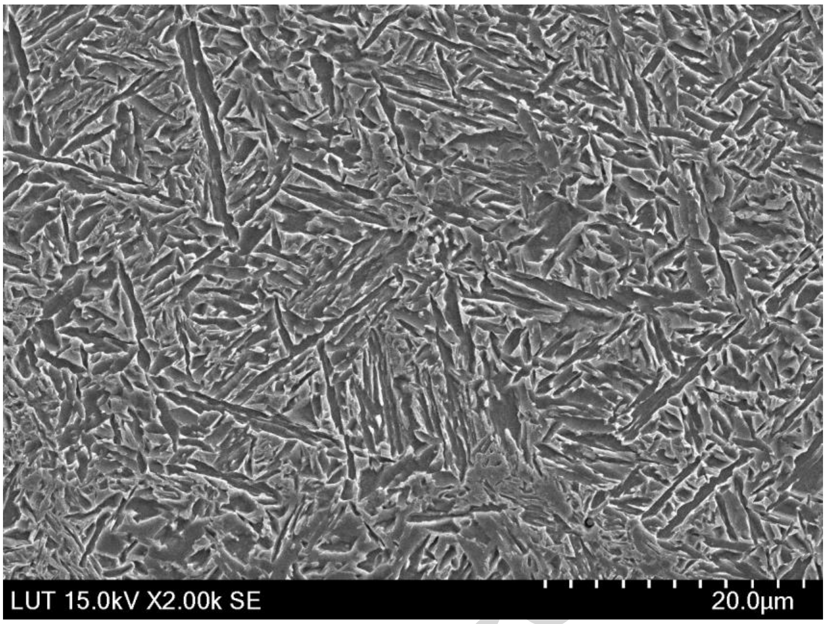

Figure 6. Microstructure of the weld metal in S700MC welded joints (Böhler alform® 700-MC).

Regarding the softened sub-zones (points 1 and 2 in figure 5.A), the microstructure of these regions was a mixture of four distinctive features. The first was the presence of blocks of a martensitic phase with a non-etched and smooth appearance, which, according to Navarro-López et al. [44], were islands of fine-textured martensite/austenite (M/A). This feature was more frequent on the virgin side. The second feature was bainite, which was more prevalent on the cold-formed side. The third was a granular shaped feature described as granular bainite in welded HSSs and UHSSs in some literature [45] or simply just ferrite by some others [37]. Finally, blocks of retained austenite were scattered along the boundaries.

Regarding the HAZ sub-zones with the highest hardness values (points 3 and 4 in figure 5.A), these areas experienced full austenitizing and subsequent cooling due to their location which was close to the fusion line. According to figures 5.D and 5.E, the hardest HAZ sub-zone on the virgin side was a mixture of martensite and bainite, while its counterpart on the cold-formed side mainly consisted of bainite. These different microstructures resulted in the higher hardness pick values on the virgin side, due to its higher martensite content. In addition, since these sub-zones experienced similar thermal gradients, this difference between their microstructures can be attributed to the effects of prior cold-forming on the bended side of the joint.

Cold-forming results in smaller austenite grain size after austenitization. Any decrease in austenite grain size results in lower martensite start and bainite start temperatures. Thus, after austenitizing and under a constant cooling rate, a cold-formed material with a finer austenitic texture (in comparison to its virgin counterpart) can be more favourable toward austenite to bainite transformation and hinder martensite formation. This behaviour results in higher bainite to martensite ratio and consequently lower maximum hardness values for the cold-formed base metals [46-48]. In addition, according to figure 7, by increasing the DOC and pre-strains, the hardness drops in the areas adjacent to the fusion line increased consequently. This behaviour is also in agreement with the earlier evaluation.

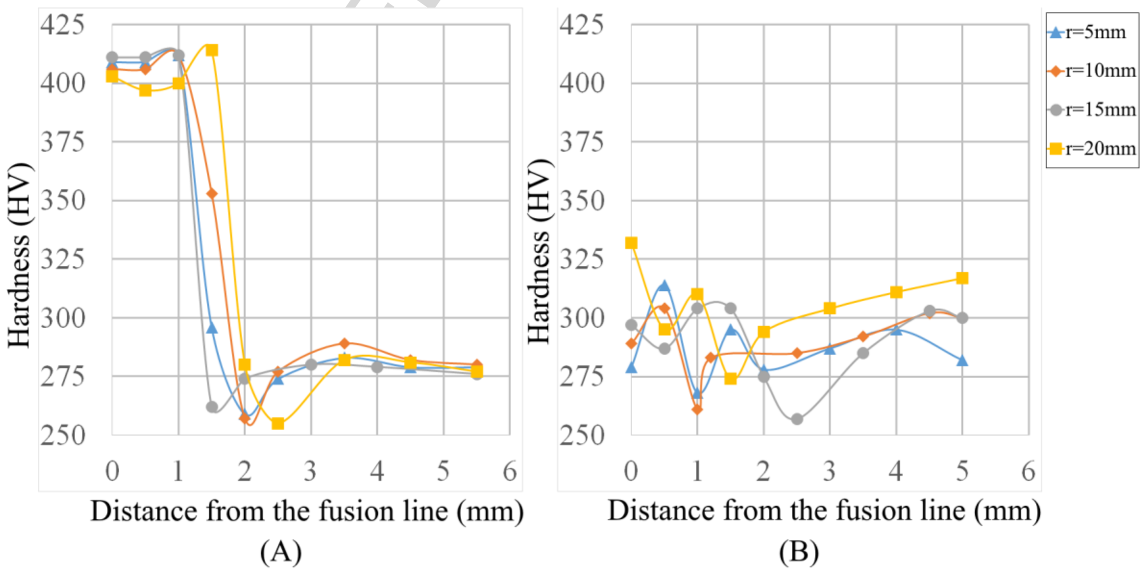

Figure 7. Hardness profiles of HAZ sub-zones on the upper sections of (A) virgin sides and (B) cold-formed sides of the samples, according to the bending radius of the cold-formed side of their joints.

Another microstructural feature near the fusion line was a feather-like ferrite, as shown in figure 8. According to this figure, the fully martensitic microstructure of the weld metal changed into a mixture of feather-like ferrite (dashed area) and islands of M/A on the fusion line. Next, the microstructure became a mixture of bainite (white arrows) and islands of M/A (black arrows) in the heat affected zone. The feathery shape (long parallel thin lines of ferrite) near the fusion line is attributed to the morphology of upper bainite in some literature [49, 50]. The appearance of upper bainite on or near the fusion line of some welded joints made from low carbon and carbon steels is expected due to the high thermal gradients and peak temperatures in these areas [51].

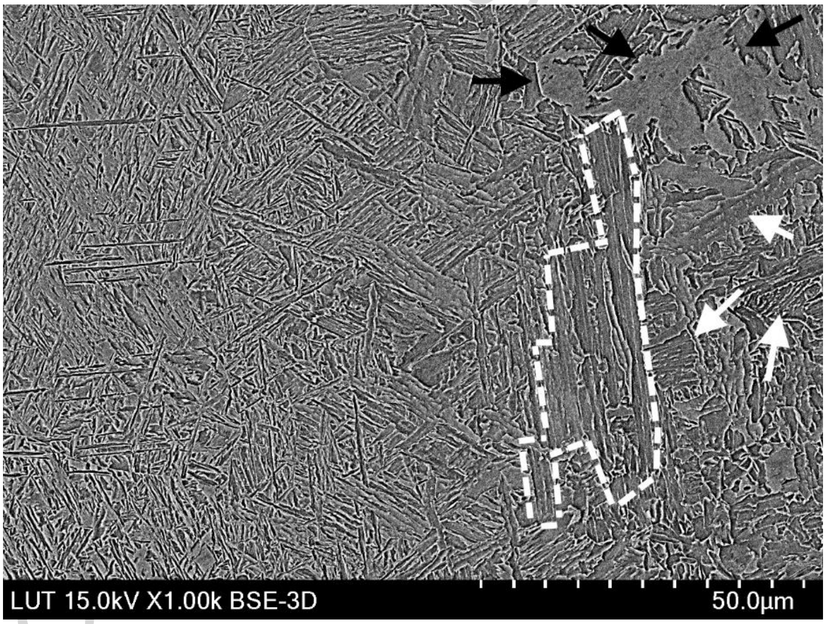

Figure 8. Microstructural features along the fusion line of the joint made from S700MC with r/t=2.

Hardness profile of the welded sample made from S1100 with *r*/*t*= 3.25 and microstructures of its HAZ sub-zones are presented in figure 9. The other S1100 samples also showed a similar trend in their hardness changes. According to this figure, the whole HAZ area generally consisted of a mixture of martensite and bainite containing sparse islands of tempered martensite. However, texture size of these features for each sub-zone was different from the other ones. Softened sub-zones (points 1 and 2 in figure 9.A) had a coarse texture which resulted in their low hardness values, while points with maximum hardness values (point 3 and 4 in figure 9.A) had a normalized microstructure which consisted of a fine-textured mixture of bainite and martensite. Unlike S700MC, hardness values of the weld metal were not significantly higher than the base materials. This behaviour can be attributed to the similarity of their microstructures. The microstructure of the weld metal (Union X96) is presented in figure 10. According to this figure, it was a mixture of bainite and martensite, similar to S1100 microstructure.

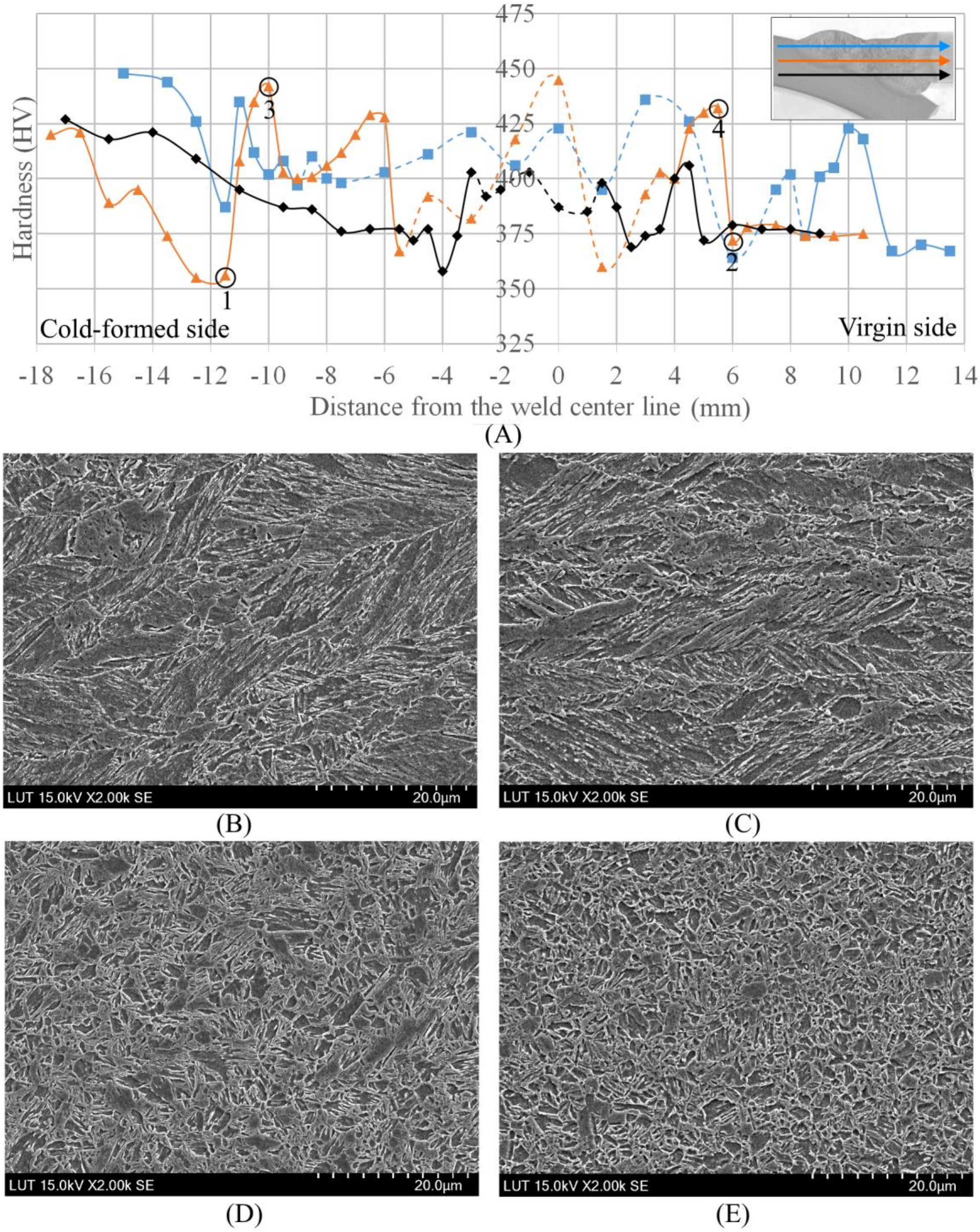

Figure 9. (A) Hardness profiles of S1100 with r/t=3.25 (weld metals are indicated by dashed lines along the profiles); and their HAZ microstructures: (B) microstructure of the softened zone on the cold-formed side (point 1 in A); (C) microstructure of the softened zone on the virgin side (point 2 in A); (D) microstructure of the point with the highest hardness value on the cold-formed side (point 3 in A); (E) microstructure of the point with highest hardness value on the virgin side (point 4 in A).

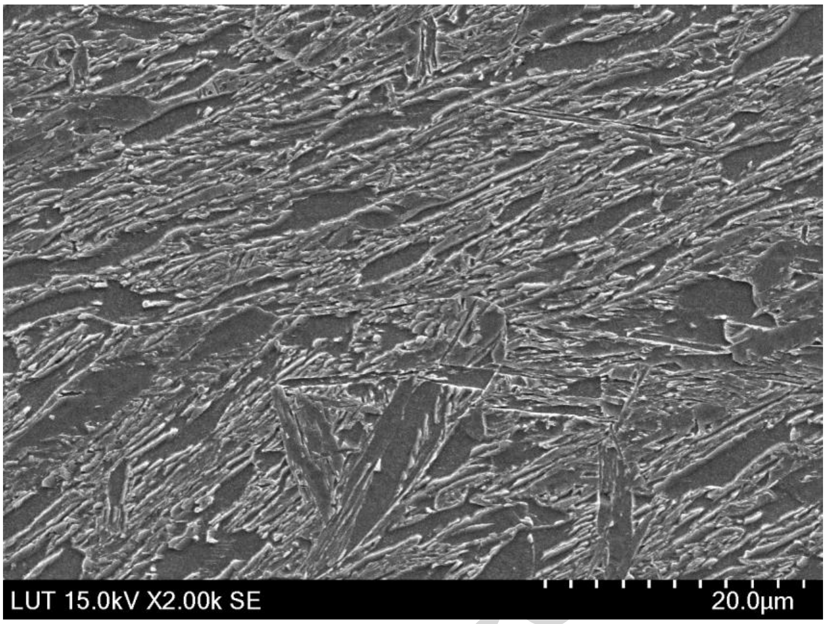

Figure 10. Microstructure of the weld metal for S1100 welded joints (Böhler Union X96).

Hardness profiles of HAZs for welded samples with different DOCs are presented in figure 11. According to this figure, hardness drops and fluctuations in the samples did not show any specific trend; however, similar to S700MC, the welded sample with the highest DOC (r=24 mm and r/t=3) had the most drastic hardness drop near the fusion line in its cold-formed base metal. According to figure 12, microstructures of the HAZs were similar to the base metals even along the fusion line, and these microstructures consisted of islands of tempered martensite (dashed areas) and martensite scattered through a bainitic background.

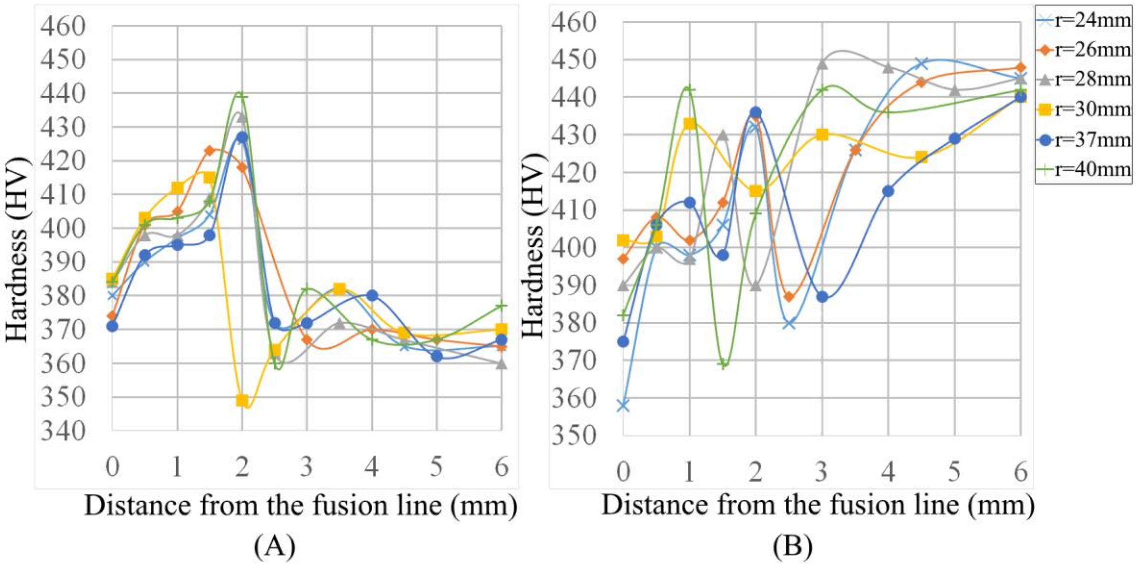

Figure 11. Hardness profiles of HAZ sub-zones on the upper sections of (A) virgin sides and (B) cold-formed sides of all the samples.

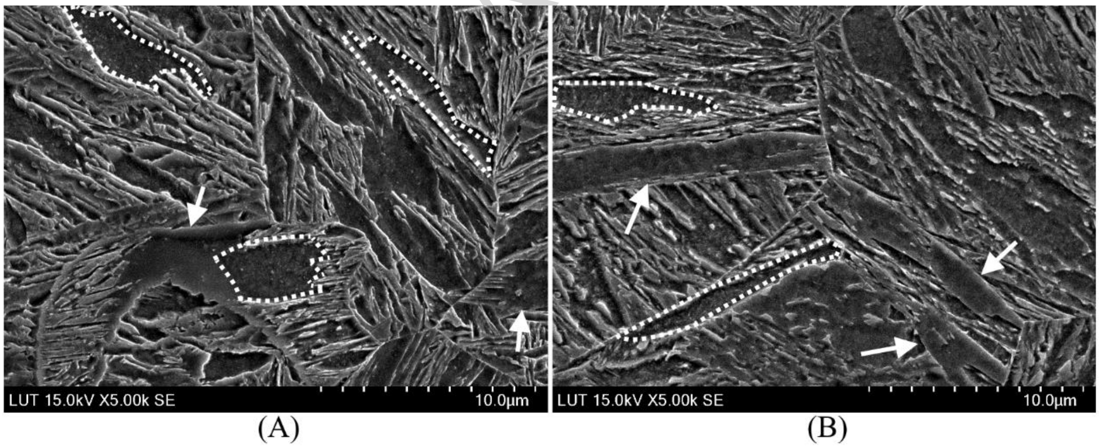

Figure 12. Microstructural features near the fusion line: (A) on the final pass of the welding in the cold-formed side (B) on the second pass in the virgin side (welded S1100, r/t = 3.25). Dashed areas are tempered martensite, while M/A islands are indicated by white arrows based on their non-etched and smooth appearance. Background phase is bainite.

3.3 Static mechanical properties

All the samples failed from their base metals in uniaxial tensile tests. As an example, DIC results and images of the fractured specimens with the highest *r*/*t* values for each base material are presented in figure 13. Results of the uniaxial tensile tests of S700MC are summarized in table 6, and their true stress-strain curves are presented in figure 14. Regarding S700MC, the welded sample with *r*/*t*=2 failed from its virgin side, while the rest, with higher DOCs and lower *r*/*t*, failed from their bended base materials. In other words, samples with DOCs higher than the recommended value (*r*/*t*=1.6 in table 3) failed from their cold-formed base material. According to table 6, samples which failed from their bended side had slightly higher yield strengths but lower elongations. However, according to figure 14, stress-strains curves of the samples were not significantly different from each other, regardless of the location of their failure.

r/t on the deformed side of the weld	Yield strength (MPa)	Tensile strength (MPa)	Fracture displacement (mm)	Elongation (%)	Approximate Young's modulus (GPa)	Area of fracture
0.5	800	844	6.9	13.8	240	Cold-formed base metal
1.0	812	864	7.0	14.0	240	Cold-formed base metal
1.5	815	880	6.9	13.8	225	Cold-formed base metal
2.0	795	871	7.6	15.2	225	Virgin base metal

Table 6. Static mechanical properties of the welded S700MC samples.

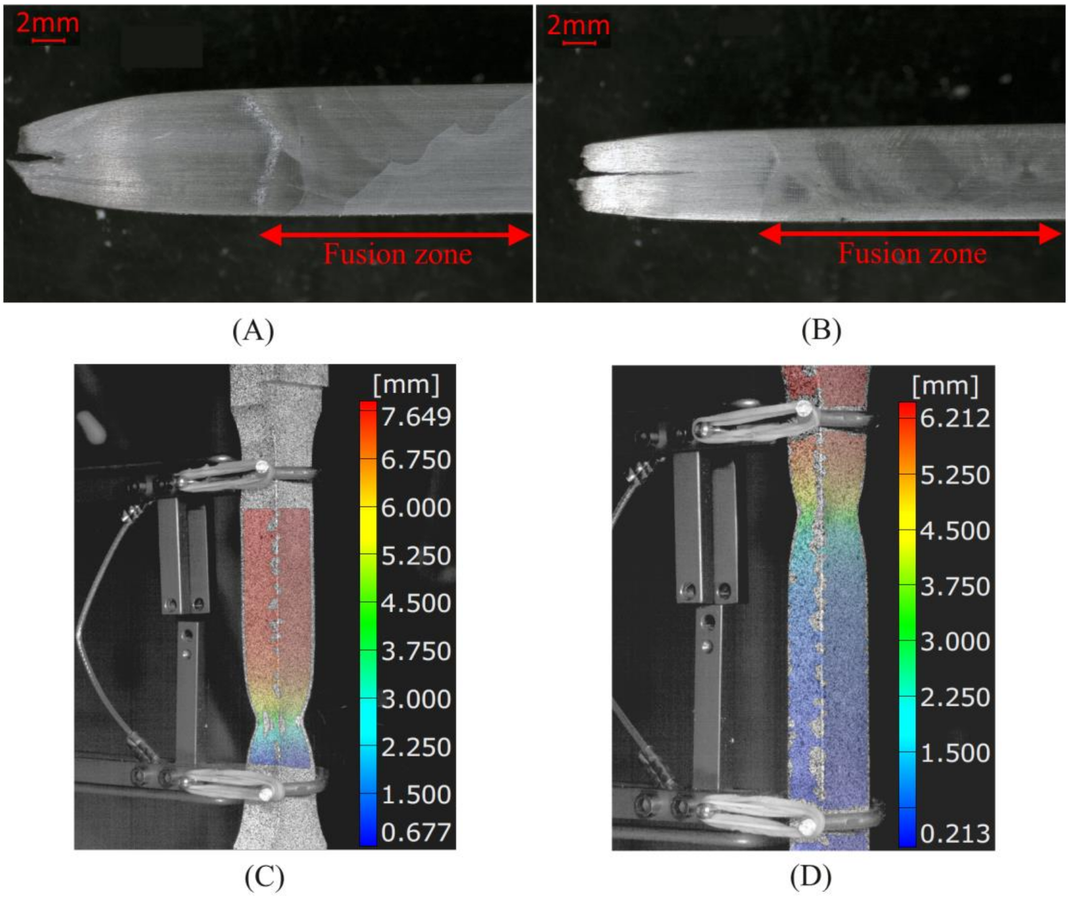

Figure 13. Fractured specimens and their DIC images just before the moment of their failures; (A) and (C): S700MC with r/t= 2; (B) and (D) S1100 with r/t= 5.

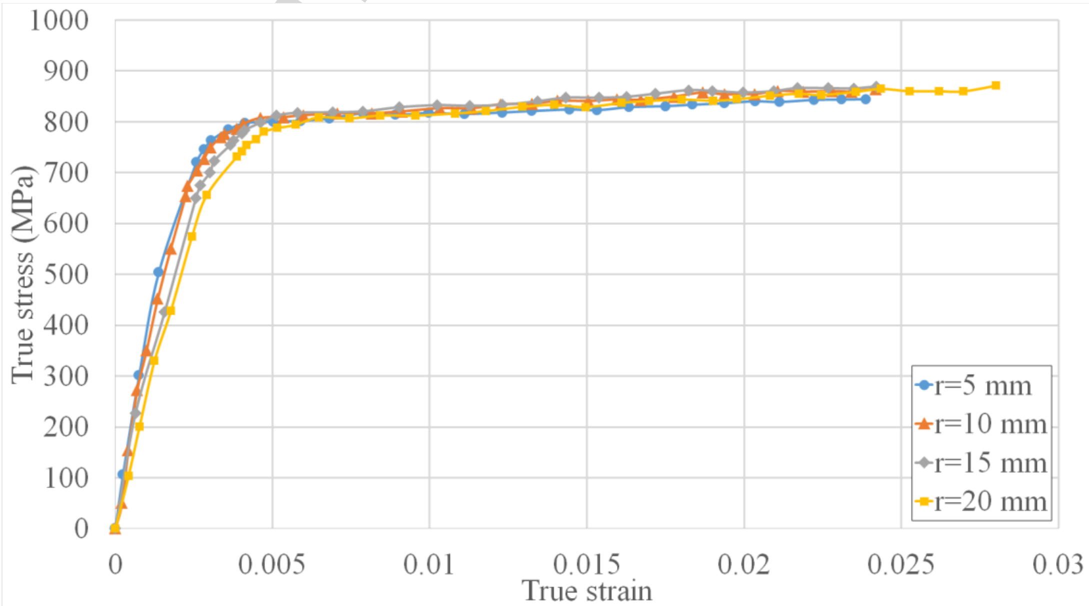

Figure 14. True stress-strain curves of the welded S700MC samples up to their necking points, according to the bending radius of their bended base metals.

Regarding S1100, the results of its uniaxial tensile tests and the true stress-strain curves are presented in table 7 and figure 15 respectively. Since all the specimens failed from their virgin base metals, all the results presented in the table and the figure represent solely one material, which is virgin S1100. Thus, regardless of the DOCs of the bended sides, the results do not show any significant variations from each other. Furthermore, these values do not represent the mechanical properties of the bended base metals.

Occurrence of failures from the virgin base metals can be attributed to the proper bending radii (or DOC) of the cold-formed materials since all of them were bended following the manufacturer's recommendation ($r/t \geq 3$). Additionally, none of the joints failed from their weld metals, although they were welded by an undermatching filler material. This result indicated the fact that stress bearing capacity of Böhler Union X96 was higher than the nominal yield strength of its weld metal in this study. Finally, it should be noted that bended S1100 base metals with $r/t \leq 3$ ruptured after bending and were not eligible for further welding procedure.

r/t on the deformed side of the weld	Yield strength (MPa)	Tensile strength (MPa)	Fracture displacement (mm)	Elongation (%)	Approximate Young's modulus (GPa)	Area of fracture
3.00	1030	1184	6.4	12.8	185	Virgin base metal
3.25	1095	1152	6.0	12.0	165	Virgin base metal
3.50	1115	1195	6.0	12.0	180	Virgin base metal
3.75	1080	1149	5.7	11.4	190	Virgin base metal
4.60	1110	1209	5.7	11.4	190	Virgin base metal
5.00	1090	1192	6.2	12.4	180	Virgin base metal

Table 7. Static mechanical properties of the S1100 welded samples.

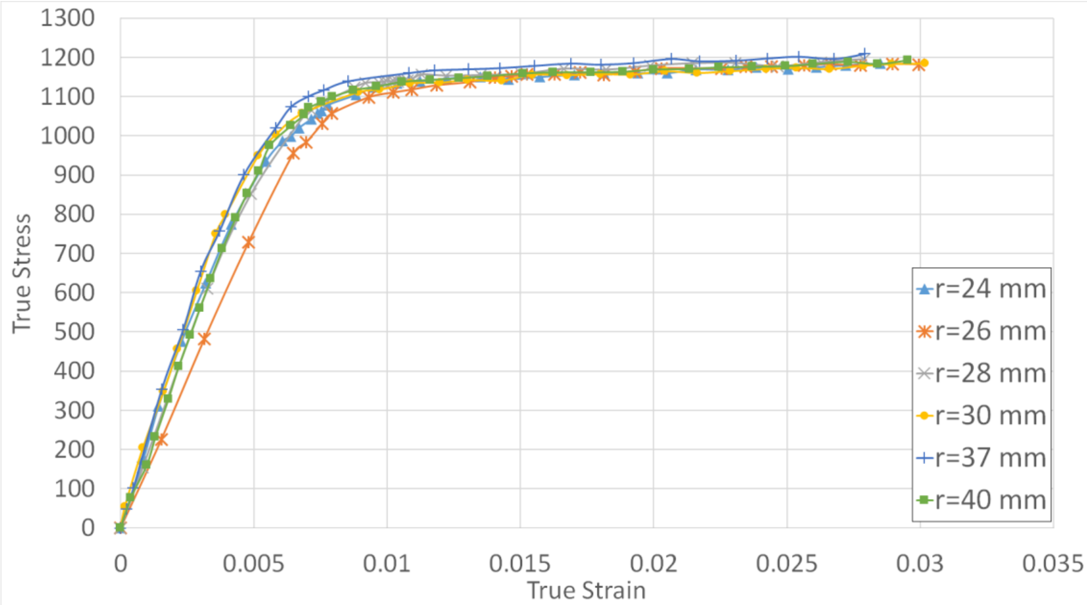

Figure 15. True stress-strain curves of the welded S1100 specimens up to their necking points, according to the bending radius of their bended base metals.

According to tables 6 and 7, there were some variations in the values of Young's modulus measured by tensile test. The fluctuations might be due to inhomogeneity of the materials throughout the gauge area of the samples. Until the yield point, the elastic displacement belonged to the whole gauge area consisting of different materials: cold-formed base metal, weld metal, virgin base metal, and heat affected zones. Thus, the overall value for Young's modulus achieved via tensile test was a combination of different moduli belonging to the dissimilar materials which led the variations in the values of Young's modulus. After the yield point, plastic deformation was focused on one spot which was the weakest material along the gauge area.

3.4 Notch toughness

In this study, Charpy impact tests were carried out with notch positions in the HAZs (1 mm away from the fusion line and into the bended material) and cold-formed base metals (5 mm away from the fusion line). The results are summarized in figure 16.

According to this figure, notch toughness values of the bended base metals increased by increasing their *r*/*t* (decreasing their DOC), as expected according to [29] and [30]. Analysis of the fractured surfaces also led to the same conclusion. As shown in figures 17 and 18, samples with higher DOCs had smaller proportions of shear fracture area (SFA). Having a smaller SFA value is an indicator of a more brittle fracture in a Charpy sample.

Based on the samples geometry (figure 1.B), correction factor from equation 2 is equal to 2. By means of this factor, bended samples with higher DOCs (*r*/*t*= 0.5 for S700MC; *r*/*t*= 3, 3.25, and 3.5 for S1100) estimated to have notch toughness values lower than the acceptance criteria provided by the manufacturer (27 J at -40 °C). Thus, welding the cold-formed sections with these *r*/*t* ratios is not recommended, especially for low-temperature applications.

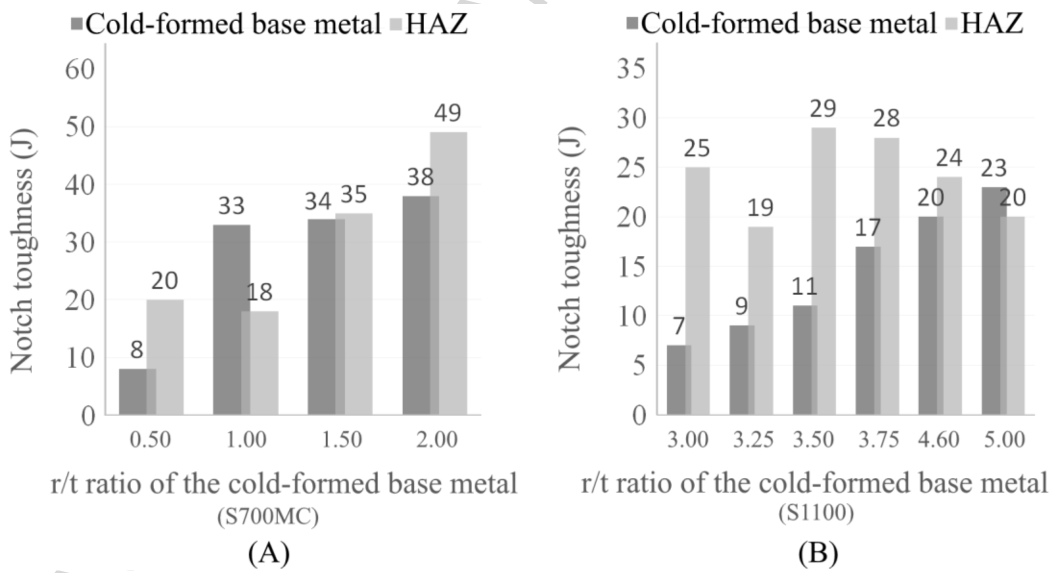

Figure 16. Notch toughness of the cold-formed base metals and their HAZs: (A) made from S700MC, and (B) made from S1100.

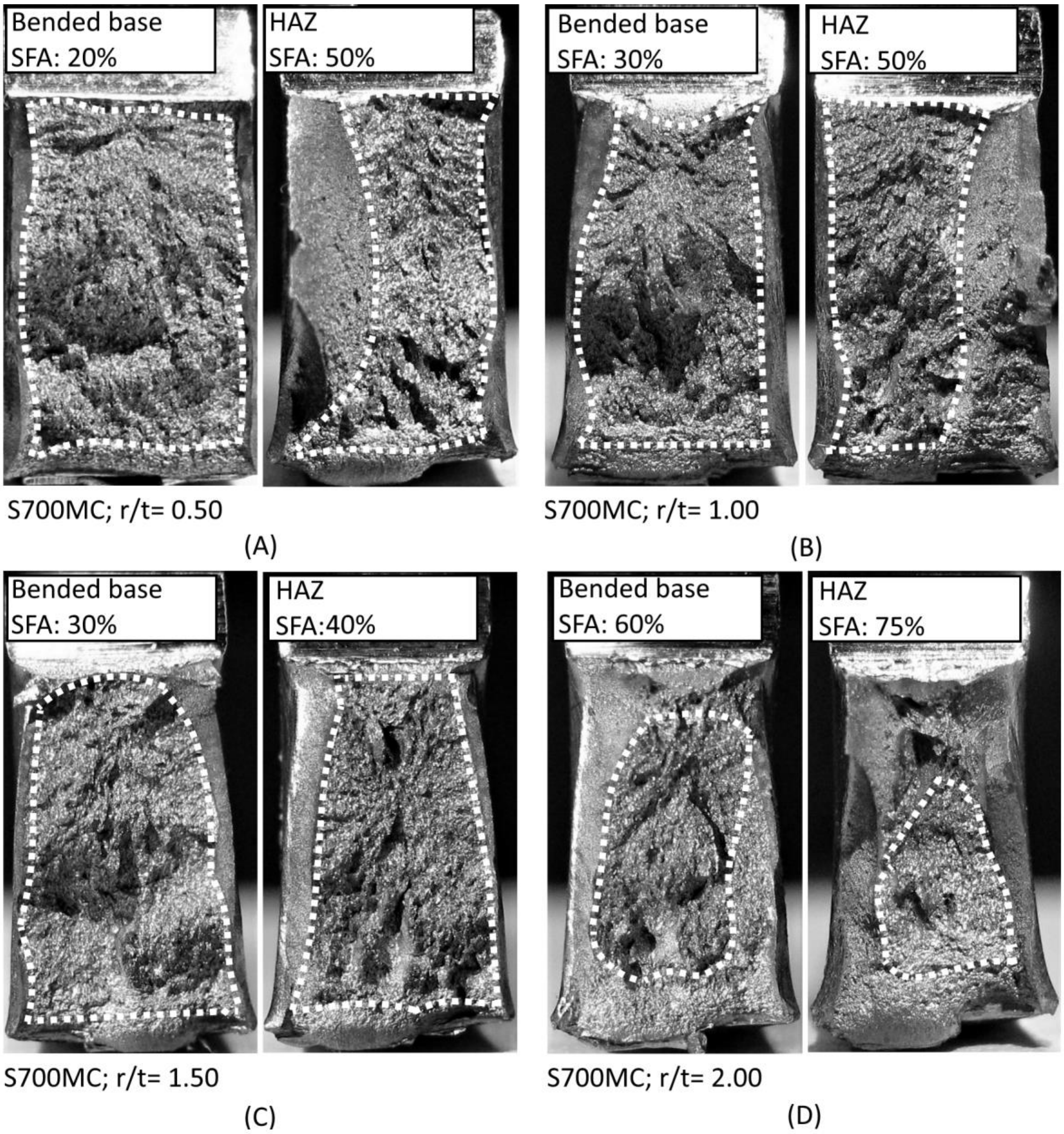

Figure 17. Fracture surfaces and their SFAs for the bended sides of the welded joints made from S700MC, according to their bending radius: (A) r = 5 mm, (B) r = 10 mm, (C) r = 15 mm, (D) r = 20 mm. Brittle fracture areas are inside the white dashed boundaries.

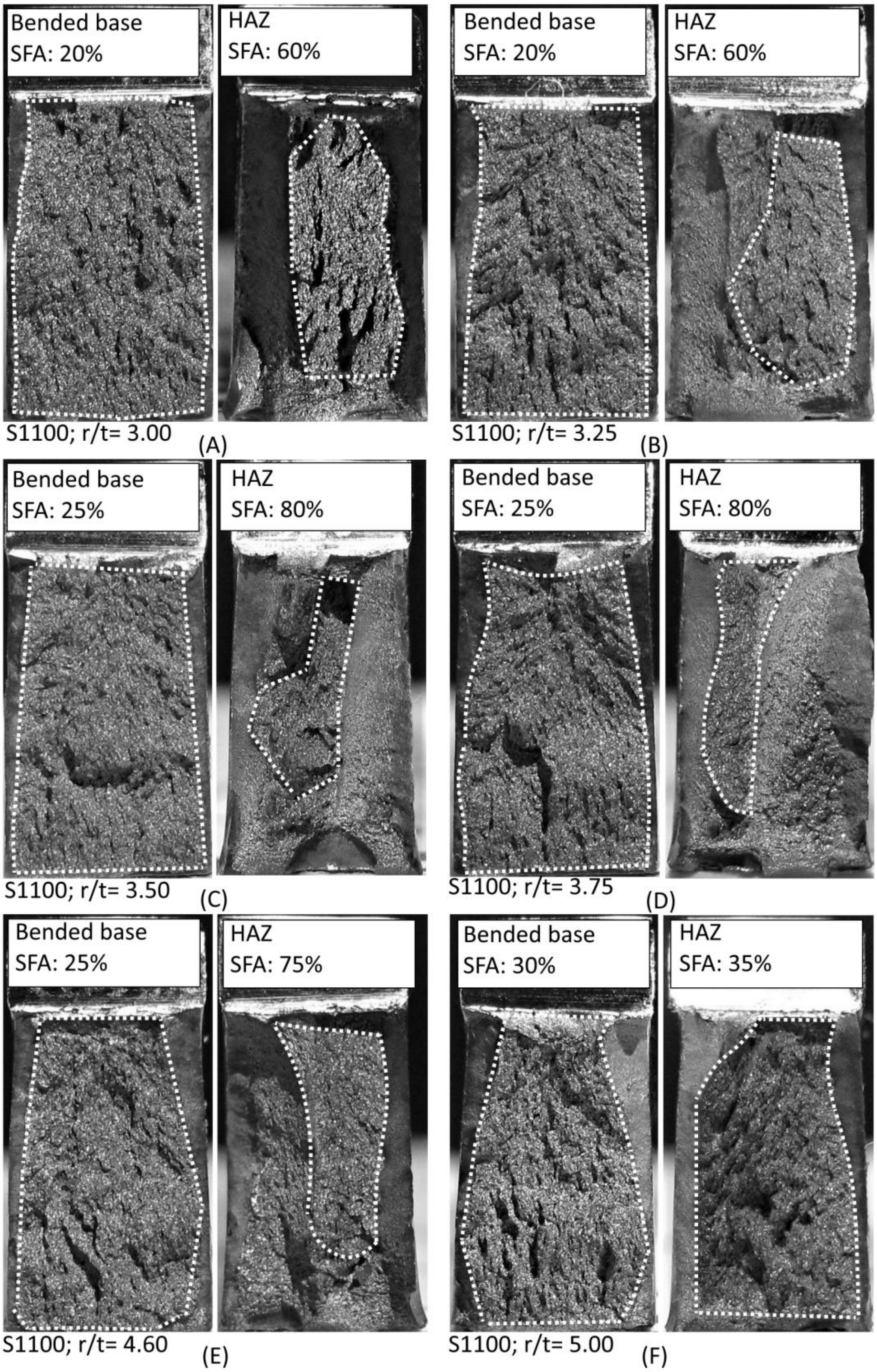

Figure 18. Fracture surfaces and their SFAs for the bended sides of the joints made from S1100, according to their bending radius: (A) r = 20 mm, (B) r = 24 mm, (C) r = 28 mm, (D) r = 30 mm, (E) r = 37 mm, (F) r = 40 mm. Brittle fracture areas are inside the white dashed boundaries.

3.5 Evaluation of the weldabilities

In this study, four criteria were considered to evaluate the weldability of cold-formed S700MC and S1100, which were their microstructures, hardness profiles, tensile properties, and fracture notch toughness values. Regarding the microstructure, S1100 did not have any harmful phases along its HAZs and in the base metal after the welding, except for some small amounts of tempered martensite. However, size and distribution of the islands of tempered martensite were not significant enough to show any negative effects on the static mechanical properties of the welded joints. For S700MC, although some undesirable phases, such as upper bainite and tempered martensite, were scattered from the fusion lines into their HAZs, they were not too defective to alter the mechanical properties. Some studies attribute the neutrality of these phases on the mechanical properties of welded joints to the low carbon content of HSSs and UHSSs [51].

Regarding the hardness values, softening occurred in all the welded samples (figures 7 and 11). In addition, it occurred more severely in their cold-formed base metals. However, since none of the samples failed from their HAZs, softening seemed to have no negative effect on the static mechanical properties of the welded joints.

Results of the uniaxial tensile tests showed the negative effect of excessive DOC on the weldabilities. According to the results, samples with bending radii smaller than the recommended values fractured from their cold-formed base metals. Results of the Charpy impact tests also led to a similar conclusion for S700MC. The results suggested even more restrictive criteria for S1100. Considering the notch toughness as the weldability measure, welded joints with r/t higher than 3.5 had an acceptable weldability.

4. Conclusions

This study investigated microstructures and mechanical properties of cold-formed S700MC and S1100 after welding to evaluate their weldability. According to the results, following conclusions can be made:

1- Generally, both S700MC and S1100 had bainitic-martensitic microstructures in their as-received and cold-formed conditions.
2- All welded samples showed patterns of hardness profiles typical for HSSs and UHSSs, including soft zones and sub-regions with the highest hardness values located near the fusion lines.
3- Hardness values were higher on the cold-formed sides of the welded joints in comparison to their virgin counterparts.
4- According to the tensile tests, welded joints with excessive DOCs fractured from their cold-formed base metals. In addition, their notch toughness was lower than acceptable values.

In conclusion, cold-formed S700MC and S1100 showed acceptable weldability and satisfactory mechanical properties after welding. However, the degree of cold-forming was a determining factor in their post welding behaviour. Excessive deformation and pre-strains resulted in premature failures in the cold-formed side of the welded joints. Regarding this matter, following the deformation limits and criteria provided by the manufacturer are highly recommended.

For further study, weldability of cold-formed S700MC and S1100 can be investigated by other typical welding techniques, such as shielded metal arc welding. In addition, other types of UHSSs with higher strengths are yet to be studied.

REFERENCES

[1] H. Aksel and Ö. Eren. 2015, "A discussion on advantages of steel structures in the context of sustainable construction", International Journal of Contemporary Architecture, vol. 2, no. 3, pp. 47-53, DOI: 10.14621/tna.20150405.

[2] A. Porter. 2015, "Weldable high-strength steels: Challenges and engineering applications", IIW International Conference, Helsinki, pp. 1-14.

[3] S. Mandal, N. K. Tewary, S. K. Ghosh, D. Chakrabarti and S. Chatterjee. 2016, "Thermo-mechanically controlled processed ultrahigh strength steel: Microstructure, texture and mechanical properties", Materials Science and Engineering: A, vol. 663, pp. 126-140, DOI: 10.1016/j.msea.2016.03.127.

[4] S. K. Maity and R. Kawalla. 2011, "Ultrahigh strength steel: Development of mechanical properties through controlled cooling", in: "Heat transfer engineering applications", V. Vikhrenko, Intech, pp. 309-337, DOI: 10.5772/26514

[5] H. Spindler, M. Klein, R. Rauch, A. Pichler and P. Stiaszny. 2005, "High strength and ultra high strength hot rolled steel grades-Products for advanced applications", Proceedings of Super-high Strength Steels, Associazione Italian di Metallurgica, Rome, pp. 1-19,

[6] S. Keeler, K. Menachem and P. J. Mooney. 2017, "Today's AHSS", in: "Advanced High Strength Steels Application Guidelines Version 6.0", WorldAutoSteel, p. 12.

[7] P. Kah, M. Pirinen, R. Suoranta and J. Martikainen. 2014, "Welding of ultra high strength steels", Advanced Materials Research, vol. 849, pp. 357-365, DOI: 10.4028/www.scientific.net/AMR.849.357.

[8] W. Guo, D. Crowther, J. A. Francis, A. Thompson, A. Liu ja L. Li, 2015, "Microstructure and Mechanical Properties of Laser Welded S960 High Strength Steel", Materials and Design, vol. 85, pp. 534-548, DOI: 10.1016/j.matdes.2015.07.037.

[9] W. Guo, Q. Liu, J. A. Francis, D. Crowther, A. Thompson, Z. Liu and L. Li, 2015, "Comparison of laser welds in thick section S700 high-strength steel manufactured in flat

(1G) and horizontal (2G) positions", CIRP Annals, vol. 64, no. 1, pp. 197-200, DOI: 10.1016/j.cirp.2015.04.070

[10] W. Guo, L. Li, D. Crowther, S. Dong, J. A. Francis and A. Thompson, 2016, "Laser Welding of High Strength Steels (S960 and S700) with Medium Thickness", Journal of Laser Applications, vol. 28, no. 2, pp. 1-12, DOI: 10.2351/1.4944100

[11] W. Guo, D. Crowther, J. A. Francis, A. Thompson and L. Li, 2016, "Process-parameter interactions in ultra-narrow gap laser welding of high strength steels", The International Journal of Advanced Manufacturing Technology, vol. 84, no. 9-12, pp. 2547-2566, DOI: 10.2351/1.4944100

[12] W. Guo, L. Li, S. Dong, D. Crowther and A. Thompson, 2017, "Comparison of microstructure and mechanical properties of ultra-narrow gap laser and gas-metal-arc welded S960 high strength steel", Optics and Lasers in Engineering, vol. 91, pp. 1-15, DOI: 10.1016/j.optlaseng.2016.11.011

[13] S. Němeček, T. Mužík and M. Míšek, 2012, "Differences between laser and arc welding of HSS steels", Physics Procedia, vol. 36, pp. 67-74, DOI: 10.1016/j.phpro.2012.10.015

[14] J. H. Lee, S. H. Park, H. S. Kwon, G. S. Kim and C. S. Lee, 2014, "Laser, tungsten inert gas, and metal active gas welding of DP780 steel: comparison of hardness, tensile properties and fatigue resistance", Materials and Design, vol. 64, pp. 559-565, DOI: 10.1016/j.matdes.2014.07.065

[15] J. Siltanen, S. Tihinen and J. Kömi, 2015, "Laser and laser gas-metal-arc hybrid welding of 960 MPa direct-quenched structural steel in a butt joint configuration," Journal of Laser Applications, vol. 27, no. S2, pp. 1-9, DOI: 10.2351/1.4906386

[16] H. Tasalloti, P. Kah and J. Martikainen, 2017, "Effect of heat input on dissimilar welds of ultra high strength steel and duplex stainless steel: Microstructural and

compositional analysis", Materials Characterization, vol. 123, pp. 29-41, DOI: 10.1016/j.matchar.2016.11.014

[17] I. Garašić, A. Ćorić, Z. Kožuh and I. Samardžić, 2010, "Occurrence of cold cracks in welding of high-strength S960 QL steel", Tehnički vjesnik, vol. 17, no. 3, pp. 327-335.

[18] A. Kurc-Lisiecka, J. Piwnik and A. Lisiecki, 2017, "Laser Welding of New Grade of Advanced High Strength Steel STRENX 1100 MC", Archives of Metallurgy and Materials, vol. 62, no. 3, pp. 1651-1657, DOI: 10.1515/amm-2017-0253

[19] F. Farrokhi, J. Siltanen and A. Salminen, 2015, "Fiber laser welding of direct-quenched ultrahigh strength steels: evaluation of hardness, tensile strength, and toughness properties at subzero temperatures", Journal of Manufacturing Science and Engineering, vol. 137, no. 6, pp. 1-10, DOI: 10.1115/1.4030177

[20] F. Javidan, A. Heidarpour, X. L. Zhao and C. R. Hutchinson, J. Minkkinen, 2016, "Effect of weld on the mechanical properties of high strength and ultra-high strength steel tubes in fabricated hybrid sections", Engineering Structures, vol. 118, pp. 16-27, DOI: 10.1016/j.engstruct.2016.03.046

[21] B. Gerhards, U. Reisgen and S. Olschok, 2016, "Laser welding of ultrahigh strength steels at subzero temperatures", Physics Procedia, vol. 83, pp. 352-361, DOI: 10.1016/j.phpro.2016.08.037

[22] Y. Peng, X. Peng, X. Zhang, Z. Tian and T. Wang, 2014, "Microstructure and mechanical properties of GMAW weld metal of 890 MPa class steel", Journal of Iron and Steel Research, vol. 51, no. 5, pp. 539-544, DOI: 10.1016/S1006-706X(14)60084-4

[23] P. Ritakallio and T. Björk, 2014, "Low- temperature ductility and structural behaviour of cold- formed hollow section structures–progress during the past two decades", Steel construction, vol. 7, no. 2, pp. 107-115, DOI: 10.1002/stco.201410024.

[24] Z. Hamedon, K. Mori and Y. Abe, 2014, “Hemming for joining high strength steel sheets”, Procedia Engineering, vol. 81, pp. 2074-2079, DOI: 10.1016/j.proeng.2014.10.288.

[25] M. Shome and M. Yumuluru, 2015, “Introduction to welding and joining of advanced high-strength steels (AHSS)” in: “Welding and Joining of Advanced High Strength Steels (AHSS)”, M. Shome and M. Yumuluru, Cambridge, Woodhead publishing, pp. 1-8, DOI: 10.1016/b978-0-85709-436-0.00001-1.

[26] P. A. Sloof and R. M. Schuster, 2000, “Yield Strength Increase of Cold Formed Sections Due to Cold Work of Forming”, 15th International Specialty Conference, Rolla, pp. 517-535.

[27] R. Arreola-Herrera, A. Cruz-Ramírez, M. Á. Suárez-Rosales and R. G. Sánchez-Álvarado, 2014, “The effect of cold forming on structure and properties of 32 CDV 13 steel by radial forging process”, Materials Research, vol. 17, no. 2, pp. 445-450, DOI: 10.1590/s1516-14392014005000041.

[28] V. Ochodek and P. Boxan, 2014, “Weldability of carbon steel processed by multiple plastic deformation”, Archives of Materials Science and Engineering, vol. 69, no. 2, pp. 88-93.

[29] A. Cosham, P. Hopkins and A. Palmer, 2004, “An experimental and numerical study of the effect of pre-strain on the fracture toughness of line pipe steel”, International Pipeline Conference, Alberta, pp. 1635-1652, DOI: 10.1115/IPC2004-0085.

[30] J. Ma, T. Chan and B. Young, 2015, “Material properties and residual stresses of cold-formed high strength steel hollow sections”, Journal of Constructional Steel Research, vol. 109, pp. 152-165, DOI: 10.1016/j.jcsr.2015.02.006

[31] E. Pfeiffer and A. Kern, 2014, “Modern production of heavy plates for construction applications – controlling production processes and quality”, Steel Construction, vol. 7, no. 2, pp. 147-153, DOI: 10.1002/stco.201420020

[32] A. Kern, U. Schriever, U. Hamme and J. Hauser, 2002, “Steel the Way”, Cranes today, vol. 2, pp. 54-59.

[33] A. Kern, U. Schriever, U. Hamme and J. Hauser, 2002, ”Steel the Way: Part 2”, Cranes today, vol. 3, pp. 55-59.

[34] J. Jia, S. Yang, W. Ni and J. Bai, 2014, “Microstructure and mechanical properties of fiber laser welded joints of ultrahigh-strength steel 22MnB5 and dual-phase steels”, Journal of Materials Research, vol. 29, no. 21, pp. 2565-2575, DOI: 10.1557/jmr.2014.273.

[35] P. J. Modenesi, R. F. Fajardo, D. B. Santos, 2010, “Steel, Mictrostructure and Mechanical Property Development in the Heat Affected Zone of Ultrafine Grained HSLA”, Materials Science Forum, vol. 638-642, pp. 3704-3709, DOI: 10.4028/www.scientific.net/MSF.638-642.3704

[36] S. Frydman, Ł. Konat and G. Pękalski, 2008, “Structure and hardness changes in welded joints of Hardox steels”, Archives of Civil and Mechanical Engineering, vol. 8, no. 4, pp. 15-27, DOI: 10.1016/S1644-9665(12)60118-6

[37] J. Górka, 2016, “Microstructure and properties of the high-temperature (HAZ) of thermo-mechanically treated S700MC high-yield-strength steel”, Materiali in tehnologije, vol. 50, no. 4, pp. 617-621, DOI: 10.17222/mit.2015.123.

[38] SSAB. 2016, ”The beauty of Strenx: Stronger and Lighter”, [Online] SSAB, Available:http://www.italautocar.com/images/informazioni_tecniche/pdf/en/materials/high_strength_steel/strenx_en.pdf [Accessed 03.01.2018].

[39] Böhler Welding, 2013, “Filler Metals Bestseller for Joining Applications”, Voestalpine, pp. 236-316.

[40] ISO 6507-1:2018, 2018, “Metallic Materials. Vickers Hardness Test. Part 1: Test Method”, European Committee for Standardization.

[41] ASTM E8M-04, 2004, “Standard Test Methods for Tension Testing of Metallic Materials [Metric]”, ASTM International.

[42] ASTM E23-07a, 2007, "Standard Test Methods for Notched Bar Impact Testing of Metallic Materials", ASTM International.

[43] E. Lucon, C. N. Mc Cowan and R. L. Santoyo, 2016, "Overview of NIST Activities on Subsize and Miniaturized Charpy Specimens: Correlations with Full-Size Specimens and Verification Specimens for Small-Scale Pendulum Machines", Journal of Pressure Vessel Technology, vol. 138, no. 3, pp. 1-42, DOI: 10.1115/1.4032474.

[44] A. Navarro-López, J. Hidalgo, J. Sietsma and M. J. Santofimia, 2017, "Characterization of bainitic/martensitic structures formed in isothermal treatments below the Ms temperature", Materials Characterization, vol. 128, pp. 248-256, DOI: 10.1016/j.matchar.2017.04.007.

[45] H. Aydin, 2014, "Relationship between a bainitic structure and the hardness in the weld zone of the friction-stir welded X80 API-grade pipe-line steel", Materiali in Tehnologije, vol. 48, pp. 15-22.

[46] H. S. Yang and H. K. D. H. Bhadeshia, 2009, "Austenite Grain Size and the Martensite-Start Temperature", Scripta Materialia, vol. 60, pp. 493-495, DOI: 10.1016/j.scriptamat.2008.11.043.

[47] A. Kundu and P. C. Chakraborti, 2014, "Effect of Austenite Grain Size and Composition on Matrix Microstructure and Properties of Steel", Procedia Materials Science, vol. 5, pp. 1141-1147, DOI: 10.1016/j.mspro.2014.07.409.

[48] E. A. Goli-Oglu, L. I. Éfron and Y. D. Morozov, 2013, "Effect of Deformation Regime in Main Stages of Controlled Rolling on Pipe Steel Microstructure", Metal Science and Heat Treatment, vol. 55, no. (5-6), pp. 294-297, DOI: 10.1007/s11041-013-9622-8.

[49] H. K. Bhadeshia, 2015, "Bainite in steels: Theory and Practice", 3rd ed., CRC Press, pp. 2-4.

[50] S. Jayanti, 2018, "Bainite: Morphology and Characteristics", [Online], Available: http://www.engineeringenotes.com/metallurgy/bainite/bainite-morphology-and-characteristics-steel-metallurgy/26960 [Accessed 03.01.2018].

[51] J. Górka and S. Stano, 2018, "Microstructure and Properties of Hybrid Laser Arc Welded Joints (Laser Beam-MAG) in Thermo-Mechanical Control Processed S700MC Steel", Metals, vol. 8, no. 2, pp. 1-15, DOI: 10.3390/met8020132

- Effects of cold-forming and pre-strains on the weldability of high strength and ultra-high strength steels.
- Effects of degree of cold-forming on the mechanical properties of welded joints.
- Microstructural analysis of welded S700MC and S1100.
- Acceptance criteria for welding cold-formed S700MC and S1100.